KECK Geology Consortium
Learning Science Through Research
Published by the Keck Geology Consortium
Short Contributions
Keck Geology Consortium
Volume 37
May 2025
doi: 10.18277/AKRSG.2025.37.06

FAULT-TIP DAMAGE ZONE DEVELOPMENT DURING NORMAL FAULT PROPAGATION WITHIN THE SEVIER FAULT ZONE, SOUTHERN UTAH

LILA RYTER, Beloit College
Project Advisor: Jim Rougvie

INTRODUCTION

As a fault begins to lengthen, it propagates both horizontally and vertically, along with the damage zone surrounding it (e.g., Peacock, 2002; Long and Imber, 2011; Siler et al., 2018). The evolution of fault damage zones has been widely studied, with two competing hypotheses coming to the forefront: the width of fault damage zones increases at a constant rate with the amount of displacement that occurs (e.g. Knott, 1994; Knott et al., 1996; Beach et al., 1999; Fossen and Hesthammer, 2000; Shipton and Cowie, 2001; Childs et al., 2009; Choi et al., 2016); or that the width of fault damage zones increases rapidly before the majority of displacement occurs (e.g. Mayolle et al., 2021, 2023).

The Sevier fault zone in southern Utah contains features that are useful for studying the evolution of fault damage zones, as it contains several active faults with different amounts of displacement and fracturing as well as units that are well exposed due to the arid desert climate (Taylor et al., 2024). There is also considerable transfer zone fracturing in the area of the tip zone of the Spencer Bench segment due to the proximity to the other main fault in the central fault zone, the Mt. Carmel segment. These fractures can be studied to determine if the orientation of fractures changes depending on their proximity to the fault.

This study uses relatively new methods involving unmanned aerial vehicles (UAV), in the form of drones, and 3D modeling to study areas that cannot be reached by foot or manned vehicles. The video footage gathered by drone flights over outcrops can be used to create a series of photographs that are then mapped to create a realistic, georeferenced Structure from Motion (SfM) model (e.g., Johnson et al., 2014).

BACKGROUND

The Sevier fault zone is located in southern Utah within the Basin and Range-Colorado Plateau transition zone and is a system of steeply (approximately 75 degrees) west-dipping normal faults (Reber et al., 2001). The transition zone displays the change from the extensional deformation of the Basin and Range Province to the relative stability of the Colorado Plateau (see Figure 2 in Surpless, this volume) and is suggested to have continued to evolve since the onset of extension at 25-30 Ma (Wannamaker et al., 2001; Taylor et al., 2024).

The tip of the Spencer Bench segment was selected for study because it is so well exposed. In order to better understand the evolution of normal fault damage zones, I compare the width of a fault-tip damage zone where no displacement has occurred to the width of fault damage zones where large amounts of displacement have occurred.

METHODS

Both ground-based scanlines and virtual outcrop modeling were used to determine the spacing and orientation of the fractures within the damage zone of the faults. In the field, we measured orientations of the fractures along scanlines, and spacing was measured between each fracture perpendicular to the fracture plane. To ensure that all fractures were distinct, only those three meters or more in length were recorded.

To create 3D models of inaccessible outcrops, a drone recorded video of the outcrop. This video was then processed with VLC media player to create an overlapping series of frame captures of the area. These images were processed by Agisoft Metashape Professional version 2.1.3 to align similar points in each photo and create a realistic model of the outcrop, which was then georeferenced using Google Earth to make sure the model is spatially accurate.

Once the model is georeferenced, I set virtual scanlines along the outcrop that is being studied. Scanline spacing was determined to best capture the majority of the fractures present in the outcrop. Spacing between fractures was measured along these scanlines, although orientation of the fractures was not.

Once the spacing data were collected, fracture intensity and a modified coefficient of variation (referred to here as Cv’) (Hooker et al., 2023) were calculated. Fracture intensity is defined as the number of fractures per meter along a scanline. Cv’ (σ / M, where σ is standard deviation and M is the median) signifies how clustered the fracture population is. Hooker et al. (2023) modified the commonly used Cv (coefficient of variation) in order to remove the low-N bias of Cv.

RESULTS

I created seven models for fracture analysis. This includes three in close proximity to the Spencer Bench segment, two farther south from the fault tip, and two fully within the transfer zone or much farther south from the fault tip (Table 1). This range in locations was to ensure that a variety of settings were included and that the full extent of the damage zones could be studied.

Fracture intensity and Cv’ were calculated for each traverse in a group of scanlines, and those were used to calculate an average intensity and Cv’ for each model. A graphical representation of the fracture spacing was created to show the distribution of fractures along scanlines.

The fracture intensity of the hanging wall damage zone ranges from 0.79 m^{-1} nearest to the fault tip (Fig. 1) to 0.25 m^{-1} in a model farther away (Table 1). The intensity of the footwall damage zone ranges from 0.41 m^{-1} (Fig. 2) to 0.1 m^{-1} in the same structural locations (Table 1). Overall, fracture intensity decreases in all structural locations as the distance from the fault tip increases. In addition, Cv’ increases farther from the fault, with Cv’ below 1 in both the hanging wall and footwall closest to the fault tip, and a Cv’ above 1 farthest from the fault tip (Table 1).

TABLE 1. SCANLINE FRACTURE DATA

Model	# of Scanlines	Length of scanline (m)	Structural Location	Distance from fault tip (m)*	Average Fracture Intensity (m^{-1})	Average Cv’
9A	1	39	Footwall	30	0.41	0.56
2018 8	2	206	Footwall	65	0.10	0.95
5B/5C	7	40	Hanging wall	75	0.79	0.89
10A-1	4	69	Hanging wall	100	0.25	0.79
10A-2	3	41	Transfer zone	170	0.11	0.77
2018 4**	4	91	Transfer zone	260	0.19	1.47
3F-2	3	62	Transfer zone	630	0.09	2.31
3F-1	2	136	Process zone***	640	0.07	1.83

Note:
* Distance from fault tip is measured from the center of the scanlines to the fault core (if in proximity) or tip.
** 3 of the scanlines in model 2018 4 are SfM-based and one is ground-based, averages have been adjusted from figures for that.
*** It is unclear what part of the damage zone these traverses are within due to the distance from the fault tip, although hypothesized here that it is the process zone.

DISCUSSION

Overall, the average intensity of the hanging wall damage zone is twice that of the footwall damage zone, and four times greater than the transfer zone fracturing (Table 1). The hanging wall damage zone is also nearly twice as wide as the footwall damage zone. This can be seen in the footwall models, as they are an overview of an intact cliff face. If the footwall damage zone was wider, there would be more erosion occurring, and the cliff would not be intact. The asymmetry of the hanging wall and footwall is consistent with studies that show damage zones of faults to be asymmetric (e.g. Berg and Skar, 2005).

The damage zone width is very similar to what was recorded in the Mt. Carmel segment, which has 200-800 meters of displacement (Costa et al., 2024), whereas there is less than 2 meters of displacement at the tip of the Spencer Bench segment. The widths

Figure 1. A) Model of the hanging wall with the seven scanlines denoted by thin white lines and labeled with corresponding numbers. The fault is denoted by a yellow dashed line and the boundary of the hanging wall denoted by a dashed white line. B) A graphical representation of the fracture distribution in the hanging wall of the Spencer Bench segment. Fractures are represented by vertical black lines.

of the damage zones of the two fault segments do not scale linearly, with the Spencer Bench segment damage zone having a width of around 70 meters and the Mt. Carmel segment damage zone having a width of 150 meters. This implies that a considerable portion of damage zone evolution occurs early in a fault's displacement history and tapers off as the fault lengthens and accumulates displacement, consistent with the findings of Mayolle et al. (2021; 2023).

The Cv' recorded for the hanging wall damage zone closest to the fault is also much greater than the Cv' recorded for the footwall damage zone (Table 1). This means that the fractures are less regularly spaced, with a more clustered fracture population present along the scanlines in the hanging wall relative to the footwall. The data also show that fracturing is more clustered farther from the fault tip. This implies that the stresses that occur in front of a fault as it is propagating are targeted on smaller areas in front of the fault. This is consistent with the findings of Olson (2004); however, it is unclear how these results relate to fault geometries, which is a potential area for further research.

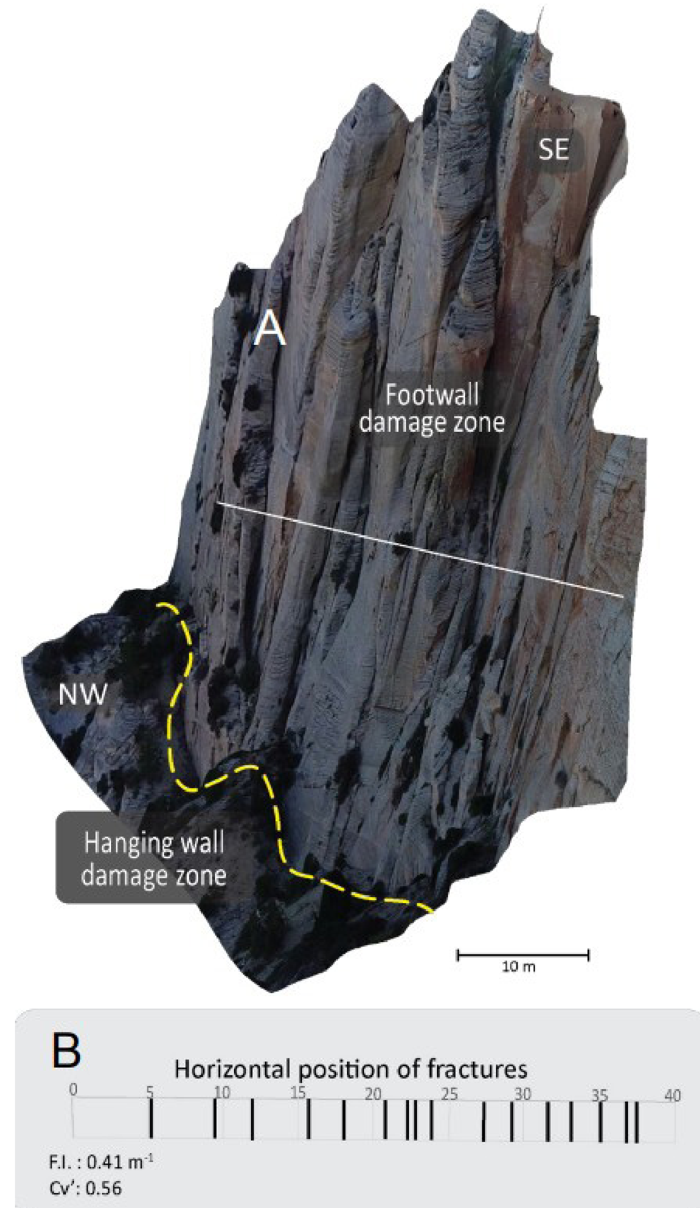

Figure 2. A) Model of the footwall nearest to the fault tip. B) Fracture distribution and statistics for the scanline in Figure 2A.

CONCLUSION

This study aimed to use modeling of faults to determine how the intensity of fractures changes in different structural positions. The results show that the hanging wall has more intense fracturing than the footwall and neighboring transfer zone and also has higher fracture clustering than the footwall. Similarly, the transfer zone has a higher clustering relative to the hanging wall. This means that stresses are asymmetric from hanging wall to footwall.

This study demonstrates that the faults and fracture networks that can be studied for fracture-related permeability are not only those with large displacements, but also the faults with very little displacement. It is shown here that there is as much fracturing within fault tip damage zones as fault wall damage zones. The hanging wall and footwall are also asymmetrical. These findings can be compared to other Keck studies that focus on fault zones with larger displacements to see how fault damage zone evolution might occur.

ACKNOWLEDGEMENTS

This material is based upon work supported by the Keck Geology Consortium and the National Science Foundation under Grant No. 2050697. Funding was also provided by NSF Award 2042114 to PI Surpless and the Trinity University Department of Earth and Environmental Geosciences. Thanks to my advisors Jim Rougvie and Ben Surpless for edits and guidance.

REFERENCES

Berg, S.S., and Skar, T., 2005, Controls on damage zone asymmetry of a normal fault zone: outcrop analyses of a segment of the Moab fault, SE Utah: Journal of Structural Geology, v. 27, p. 1803-1822, doi:10.1016/j.jsg.2005.04.012.

Beach, A., Welbon, A.I., Brockbank, P.J., and McCallum, J.E., 1999, Reservoir damage around faults: outcrop examples from the Suez Rift: Petroleum Geoscience, v. 5, p. 109-116, doi:10.1144/petgeo.5.2.109.

Childs, C., Manzocchi, T., Walsh, J.J., Bonson, C.G., Nicol, A., and Schopfer, M.P.J., 2009, A geometric model of fault zone and fault rock thickness variations: Journal of Structural Geology, v. 31, p. 117-127, doi:10.1016/j.jsg.2008.08.009.

Choi, J-H., Edwards, P., Ko, K., Kim, Y.S., 2016, Definition and classification of fault damage zones: A review and a new methodological approach: Earth-Science Reviews, v. 152, p. 70-87, doi:10.1016/j.earscirev.2015.11.006.

Costa, S., Montalvo, A., Ryter, L., and Surpless, B., 2024, Constraining Fault Damage Zone Evolution Within the Sevier Normal Fault System, Southern Utah: GSA Connects 2024 Meeting in Anaheim, California, 13-29 September 2024, v. 56, id.400976.

Fossen, H., 2016, Structural Geology: Cambridge University Press, Cambridge, UK, 510 p.

Fossen, H., and Hesthammer, J., 2000, Possible absence of small faults in the Gullfaks Field, northern North Sea: implications for downscaling of faults in some porous sandstone: Journal of Structural Geology, v. 22, p. 851-863, doi:10.1016/S0191-8141(00)00013-4.

Hooker, J., Marrett, R., and Wang, Q., 2023, Rigorizing the use of the coefficient of variation to diagnose fracture periodicity and clustering: Journal of Structural Geology, v. 168, 104830, doi: 10.1016/j.jsg.2023.104830.

Johnson, K., Nissen, E., Saripalli, S., Arrowsmith, R., McGarey, P., Scharer, K., Williams, P., and Blisnuik, K., 2014, Rapid mapping of ultrafine fault zone topography with structure from motion: Geosphere, v. 10, p. 969-986, doi:10.1130/GES01017.1.

Knott, S.D., 1994, Fault zone thickness versus displacement in the Permo-Triassic sandstone of NW England: Journal of the Geological Society, v. 151, p. 17-25, doi:10.1144/gsjgs.151.1.0017.

Knott, S.D., Beach, A., Brockbank, P.J., Brown, J.L., McCallum, J.E., Welbon, A.I., 1996, Spatial and mechanical controls on normal fault populations: Journal of Structural Geology, v. 18, p. 359-372, doi:10.1016/S0191-8141(96)80056-3.

Long, J., and Imber, J., 2011, Geological controls on fault relay zone scaling: Journal of Structural Geology, v. 33, p. 1790-1800, doi:10.1016/j.jsg.2011.09.011.

Mayolle, S., Soliva, R., Dominguez, S., Wibberley, C., and Caniven, Y., 2021, Nonlinear fault damage zone scaling revealed through analog modeling: Geology, v. 49, p. 968-972, doi.org/10.1130/G48760.1.

Mayolle, S., Soliva, R., Dominguez, S., and Wibberley, C., 2023, Normal fault damage zone growth in map view from analogue models: Journal of Structural Geology, v. 176, 104975, doi: 10.1016/j-jsg.2023.104975

Metashape, Agisoft, 2024. Agisoft Metashape User Manual (pdf): accessed July, 2024, https://www.agisoft.com/pdf/metashape-pro_2_1_en.pdf,

version 2.1.3.
Olson, J. E., 2004, Predicting fracture swarms - the influence of subcritical crack growth and the crack-tip process zone on joint spacing in rock, in : Cosorove, J. W. & Engelder, T., eds., The Initiation, Propagation, and Arrest of Joints and Other Fractures, London, Geological Society, Special Publications, v. 231, p. 73-87, doi: 10.1144/gsl.sp.2004.231.01.05.
Peacock, D.C.P., 2002, Propagation, interaction and linkage in normal fault systems: Earth-Science Reviews, v. 58, p. 121-142, doi:10.1016/S0012-8252(01)00085-X.
Siler, D., Hinz, N., and Faulds, J., 2018, Stress concentrations at structural discontinuities in active fault zones in the western United States: Implications for permeability and fluid flow in geothermal fields: Geological Society of America Bulletin, v. 130, p. 1273-1288, doi:10.1130/B31729.1.
Shipton, Z.K., and Cowie, P.A., 2001, Damage zone and slip-surface evolution over µm to km scales in high-porosity Navajo sandstone, Utah: Journal of Structural Geology, v. 23, p. 1825-1844, doi:10.1016/S0191-8141(01)00035-9.
Surpless, B., and McKeighan, C., 2022, The role of fracture branching in the evolution of fracture networks: An outcrop study of the Jurassic Navajo Sandstone, southern Utah: Journal of Structural Geology, v. 166, 104664, doi:10.1016/j.jsg.2022.104664
Taylor, W., Surpless, B., and Scheifelbein, I., 2024, Complex fault segment linkage within the Sevier fault zone, southern Utah: Lithosphere, 28 p. doi:10.2113/2024/lithosphere_2023_332.
Reber, S., Taylor, W.J., Stewart, Meg, and Schiefelbein, I.M., 2001, Linkage and reactivation along the northern Hurricane and Sevier faults, southwestern Utah, In Erskine, M.C., Faulds, J.E., Bartley, J.M., and Rowley, P.D., Eds, The geologic transition, High Plateaus to Great Basin—A symposium and field guide, The Mackin Volume: Utah Geological Association Publication 30, Pacific Section American Association of Petroleum Geologists Publication GB 78, p. 379-400
Wannamaker P. E., Bartley, J. M., Sheehan, A. F. et al, 2001, The geologic transition, high plateaus to Great Basin - a symposium and field guide: Utah Geological Association Publication 30 and Pacific Section American Association of Petroleum Geologists guidebook, in M.E. Erskine, J.E. Faulds, J.M. Bartley, and P.D. Rowley, Eds., Great Basin-Colorado Plateau transition in central Utah: an interface between active extension and stable interior, 78th ed., p. 1-38.